TABLE 1 Effect of the Counterclockwise Winding of the Parasitic QHA onthe Performance of the Axial Ratio and HPBW

Pitch Angle (α)	Length of Copper Wires (Normalized to λ)	With Printed Copper Strips	ResonantFrequency (GHz)	Bandwidth with AR < 3 dB (MHz)	HPBW
30°	0.936	Yes	3	81.3	54°
	0.936	No	3	40.5	38°
35°	0.75	Yes	2.67	60.3	41°
	0.75	No	2.67	20	41°
40°	0.5	Yes	3.17	80.2	39°
	0.5	No	3.17	39.9	33°
45°	0.5	Yes	3.64	170	68°
	0.5	No	3.64	40	52°
50°	0.7	Yes	2.67	55.8	79°
	0.7	No	2.67	20.8	50°

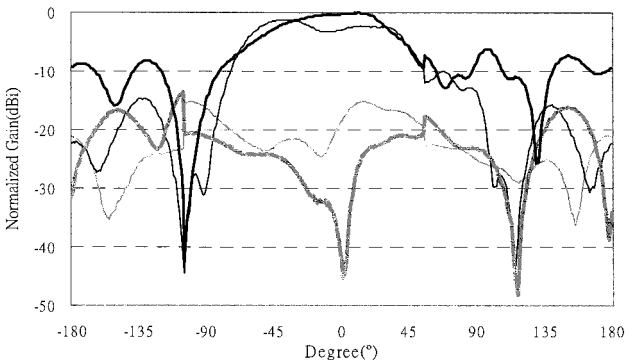

Figure 4 Radiation pattern of configurations in a counterclockwise winding at $l = 0.5\lambda$ and $\alpha = 45°$ at 3.64 GHz. ····· LHCP of the QHA with parasitic strips, ····· LHCP of the QHA without parasitic strips, —— RHCP of the QHA with parasitic strips, —— RHCP of the QHA without parasitic strips

use of a parasitic copper strip QHA is still under investigation.

4. CONCLUSIONS

A novel QHA with a second parasitic QHA is proposed and intensively studied. It is found that the return loss can be reduced from −28 to −47 dB, and the impedance bandwidth (with SWR < 2) can be broadened to 39%. The bandwidth with circular polarization can also be significantly increased. The HPBW of the radiation pattern can be increased from 53 to 68°. This compact antenna is ready for use in mobile satellite communications.

REFERENCES

1. A.T. Adams and C. Lumjiak, Optimization of the quadrifilar helix antenna, IEEE Trans Antennas Propagat (July 1971), 547–548.
2. T. Kamei, S. Takashi, H. Morishita, and T. Nagao, Quadrifilar helical antennas with a variable conical beam, 10th Int Conf Antennas Propagat, 1997, vol. 1, pp. 543–545.
3. K. Fujimoto and J.R. James, Mobile antenna systems handbook, Artech House, Norwood, MA, 1994, chap. 6.5.2, pp. 455–457, 535–536.
4. T. Hirota, A. Minakawa, and M. Muraguchi, Reduced-size branch-line and rat-race hybrids for uniplanar MMIC's, IEEE Trans Microwave Theory Tech 38 (1990), 270–275.

A STUDY OF THE FOUR-PATH MODEL FOR SCATTERING FROM AN OBJECT ABOVE A HALF SPACE

Joel T. Johnson[1]
[1] Department of Electrical Engineering and ElectroScience Laboratory
The Ohio State University
Columbus, Ohio 43210

Received 15 February 2001

ABSTRACT: *A study of scattering from a dielectric object located above a half space is performed to clarify the accuracy of a "four-path" model which includes single scattering effects only. An iterative method-of-moments solution is used for comparison, and both frequency- and time-domain examples are illustrated to clarify the scattering interactions which occur.* © 2001 John Wiley & Sons, Inc. Microwave Opt Technol Lett 30: 130–134, 2001.

Key words: *electromagnetic scattering; radar cross section*

1. INTRODUCTION

Many practical geometries for radar applications involve objects in the presence of the Earth surface. Although the ground surface typically has complex features such as vegetation, surface roughness, or dielectric constant variations, in many cases, these effects can be neglected, and the surface of the Earth can be modeled as a planar boundary between free space and a homogeneous dielectric medium. Electromagnetic scattering from objects above a half space has been studied extensively, but analytical solutions are not readily available due to the complexity of the half-space Green's function. A simple "four-path" approximate model which includes only single scattering effects has been widely applied [1–4], but the accuracy of this model has not been explored in detail. Numerical solutions which include all scattering interactions have also been developed [5–7], but insight into the scattering process is not directly provided by these techniques. An analysis of numerical model results to clarify the important scattering mechanisms would therefore be useful for improving understanding and for testing the simple four-path model.

Contract grant sponsor: ONR
Contract grant number: N00014-97-1-0541, N00014-00-1-0399
Contract grant sponsor: NSF
Contract grant number: Project ECS-9701678
Contract grant sponsor: Duke University as part of the OSD MURI on Humanitarian Demining

In this paper, an examination of the four-path model is performed through comparison with results from an efficient numerical model for scattering from a three-dimensional dielectric object in the presence of a dielectric half space. Results in both frequency and time domains are illustrated to allow distinct scattering interactions to be compared. Results show the four-path model to provide reasonable predictions, although higher order interactions are also observed in numerical model data. The following section describes the numerical model used, and Section 3 discusses the example problem considered. A description of the computational issues involved follows in Section 4, and results are presented in Section 5.

2. NUMERICAL MODEL

Figure 1 illustrates the basic geometry considered in this paper: a dielectric object with relative complex permittivity ϵ_3 is located above an interface between free space and a dielectric half space with relative complex permittivity ϵ_2. A method-of-moments formulation of this problem typically would be based on use of the half-space Green's function, so that unknowns would be required only on the dielectric object. However, the current study applies an algorithm [8] which places volumetric electric current unknowns inside the dielectric object and electric and magnetic surface current unknowns on the dielectric boundary, allowing use of the simpler unbounded medium Green's function. This model was developed for studies of scattering from objects in the presence of rough surfaces, for which the half-space Green's function formulation is invalid.

Although the current model will clearly have an increased number of unknowns when compared to a half-space Green's function method, the efficiency of the formulation still allows solutions to be obtained in a reasonable time. Computational efficiency is achieved through the use of an iterative solution of the moment-method matrix equation (using the bi-CGSTAB algorithm [9]) and through application of the canonical grid (CAG) [10–11] and discrete-dipole approximation (DDA) [12–13] methods for computing surface-to-surface and object-to-object point couplings, respectively, in order $N \log N$ computations, where N is the number of surface or object unknowns. A detailed description of the algorithm is provided in [8].

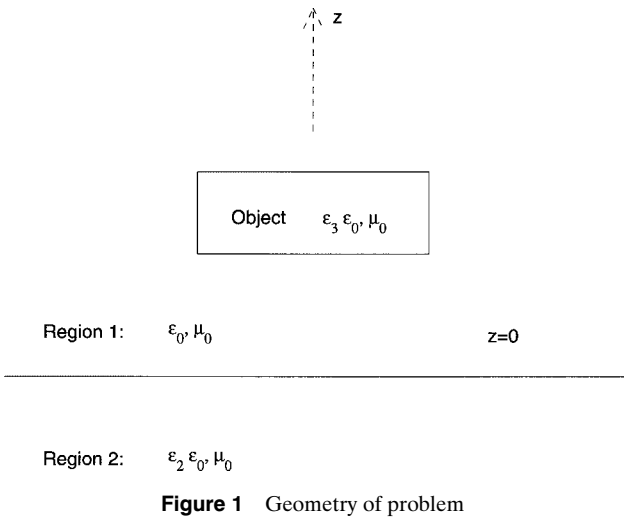

Figure 1 Geometry of problem

3. EXAMPLE PROBLEM

A dielectric rectangular box with dimensions 7.62 cm × 7.62 cm × 2.54 cm (thickness) and relative permittivity $\epsilon_3 = 3 + i0.03$ is used as the object in the results illustrated below. The center of the box is located 7.62 cm above an interface between free space and a medium with relative permittivity $\epsilon_2 = 5 + i1.25$. Scattering from this object is to be determined for a field incident at either 15 or 45° from normal incidence at frequencies from 2 to 5.1 GHz.

Because the model used places unknowns on the dielectric interface between regions one and two, the interface considered must be of finite size. A 1.28 m × 1.28 m interface is used, and artificial edge scattering effects are avoided through use of the "tapered-wave" incident field described in [14]. This field is designed to mimic an incident plane wave, but provides attenuation of incident fields as surface edges are approached. For tapering parameter $g = 3.333$, the field incident on the surface edges is approximately 24 dB lower than that at the center, and the object horizontal cross section projected onto the flat interface is well within the 3 dB incident spot size. A test of tapered-wave influence will be described below through comparison with a plane-wave incidence half-space Green's function code.

Figure 2 illustrates the scattering mechanisms considered in the approximate four-path model, which includes only a single scattering interaction with the dielectric object. Path 1 is a standard backscattering path, and is calculated as though the object were located in free space. Paths 2 and 3 involve a bistatic scatter from the object (again computed as if the object were in free space) and a reflection from the boundary, so an appropriate reflection coefficient must be included in the scattered field amplitude. Note that, since these two paths are identical under time reversal, their contributions are equal. Path 4 involves two reflections from the interface and a backscatter from the bottom surface of the object. Since the object considered in this example is symmetric in z, paths 1 and 4 involve the same object scattering coefficient. The four-path model represents scattering from an object in the presence of a dielectric boundary as the sum of these four mechanisms, including appropriate phase shifts due to the excess path lengths traveled in paths 2–4.

4. COMPUTATIONAL ISSUES

Since the 1.28 m × 1.28 m interface ranges between 8.5 and 21.76 free-space wavelengths as the frequency is varied from 2 to 5.1 GHz, the interface is sampled into 256 × 256 points in the results shown. Although this is somewhat small for the higher frequencies given that the lower medium wavelength is approximately 2.25 times shorter than that in free space, a set of comparisons using 512 × 512 points showed only slight changes in scattered cross sections. While a smaller number of points could be used for the lower frequencies, a constant number of points sampling the interface as the frequency is varied was chosen for convenience. The resulting number of field unknowns on the interface is 262,144. The object is sampled on a 32 × 32 × 8 point grid with step size 3.175 mm (ranging from approximately $1/27$ to $1/11$ of the wavelength in the object as the frequency varies), resulting in a total number of 13,824 object unknowns. The combined problem thus contains approximately 276,000 unknowns.

Although the problem considered can be solved on a PC level platform, total computing times for the multiple cases considered in this paper were further reduced through use of

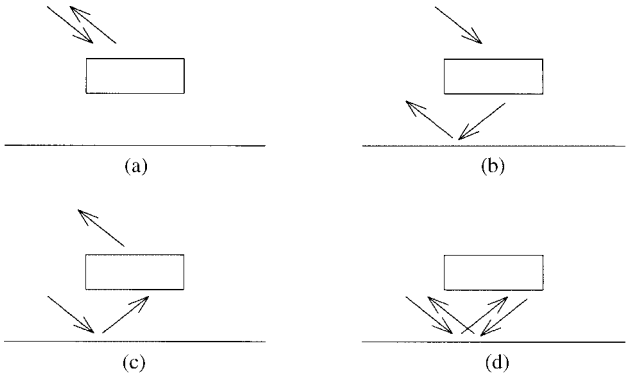

Figure 2 Scattering mechanisms of four-path model. (a) Path 1. (b) Path 2. (c) Path 3. (d) Path 4

IBM SP parallel computing resources at the Maui High Performance Computing Center [15]. Since results as a function of frequency were of interest, single-frequency calculations were performed on individual nodes of the parallel computer (comparable to PC platforms) to obtain 32 frequencies between 2 and 5.1 GHz. Single-frequency computing times on a single node were approximately 2 h; attempts to optimize computing times have, at present, not been performed extensively. Note that these times compare favorably with half-space Green's function codes due to the extensive computational time required for calculation of the half-space Green's function.

Four-path model contributions were calculated using an object in free-space DDA code [12–13] with the same grid as in the combined surface/object code. The smaller number of unknowns in the object-only problem allows a complete solution for all 32 frequencies to be obtained within 10 min on a 700 MHz Pentium III PC. The dramatic decrease in time for these computations indicates the motivation for use of the four-path model; development of approximate solutions for scattering from an object above a half space is also possible with the four-path model if an approximate theory for bistatic scattering from an object in free space is available.

5. RESULTS

Figure 3 illustrates *HH* polarized backscattering cross sections versus frequency for an incidence angle of 15°. For validation, predictions from the ESP5 half-space Green's-function-based code [16] are included for comparison at a subset of the computed frequencies; good agreement is observed, indicating that tapered-wave effects are not altering object cross sections significantly. Some discrepancies within 1 dB are observed, but are difficult to resolve due to computational limitations of the half-space code which is based on direct matrix equation solution. Results from the four-path model are also included, and show good agreement with numerical results. This comparison indicates that the four-path model captures the dominant scattering mechanisms of the problem, although discrepancies of up to 3.3 dB and an error standard deviation (in decibel values) of 1.2 dB indicate that multiple interaction effects not captured by the four-path model may be significant in some cases.

Figure 4 illustrates the same comparisons for 45° incidence and for both *HH* and *VV* cross sections. Polarization effects should be expected to become more important as the incidence angle increases due to polarized object scattering

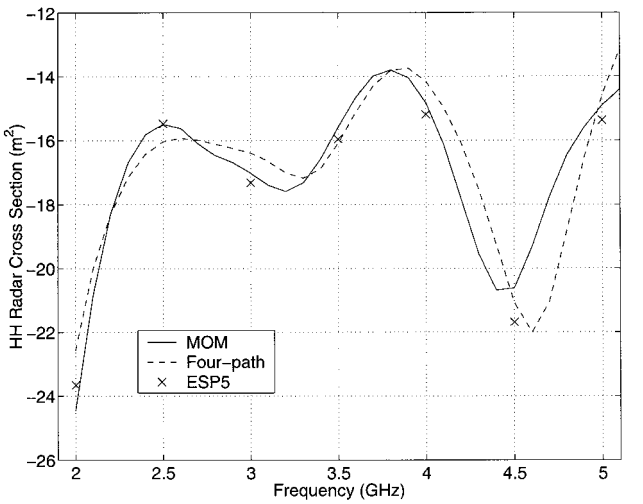

Figure 3 *HH* polarized radar cross sections versus frequency for 15° incidence. Comparison of method-of-moments solution with four-path model and ESP5 half-space Green's function solution

effects, and due to the difference between vertical and horizontal half-space reflection coefficients at larger incidence angles. Results indeed show significant differences between *HH* [plot (a)] and *VV* [plot (b)] results, and again the current model provides excellent agreement with the half-space Green's function code. The error of the four-path model increases compared to Figure 3, with maximum errors of approximately 6.5 dB for both *HH* and *VV* results, and with error standard deviations of approximately 2.1 and 2.6 dB, respectively. Note that the four-path model tends to overpredict numerical model *HH* cross sections; the mean error (again in decibel values) is 2.85 dB. These results continue to indicate that the four-path model captures dominant scattering effects, but neglects some mechanisms which may be significant,

To further explore the important scattering mechanisms, Figures 5 and 6 plot time-domain backscattered fields corre-

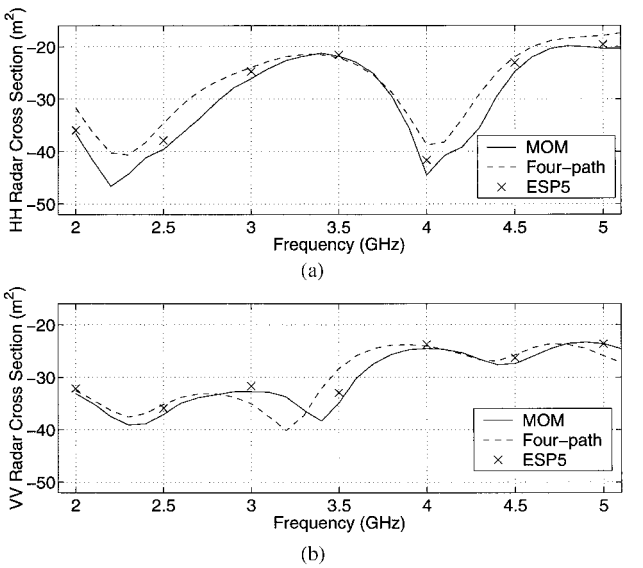

Figure 4 Radar cross sections versus frequency for 45° incidence. Comparison of method-of-moments solution with four-path model and ESP5 half-space Green's function solution. (a) *HH*. (b) *VV*

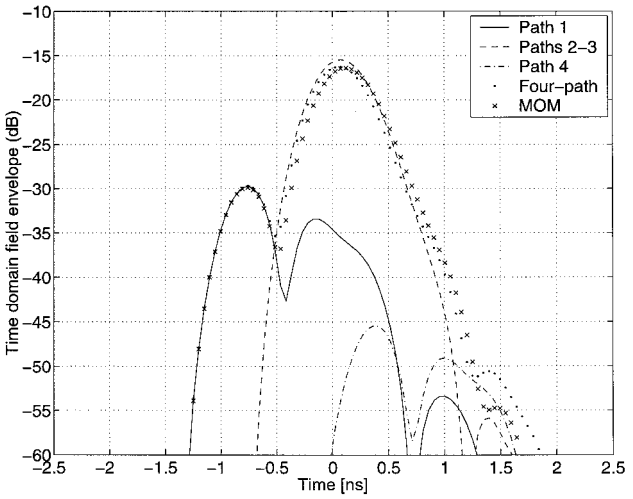

Figure 5 Envelope of *HH* time-domain backscattered fields for 15° incidence. Comparison of method of moments with four-path model

sponding to the results for Figures 3 (15° incidence) and 4 (45° incidence), respectively. The envelope of backscattered fields in decibels is illustrated in these figures, obtained from an inverse FFT after applying a Kaiser–Bessel window function with parameter $\beta = 6$. Time zero is defined at the origin of the half space, so object scattering returns appear at times less than zero. Four-path model results are included in these plots for each individual path as well as their combination; individual path results show the early time return from the object in path 1, the bistatic returns of paths 2 and 3 around time 0, and path 4 returns at longer time delays, as expected. Note in Figure 5 that the bistatic contribution of paths 2 and 3 is more significant than the direct object backscatter due to the relatively low contrast of the object, which results in the majority of energy remaining in the near-forward scattering region. In all cases, excellent agreement with numerical model results is obtained at early times where object only effects dominate scattering returns. However, some differences are observed around time zero, which become larger for the 45° cases, and particularly in vertical polarization. Longer time-delayed results show significant differences in all cases.

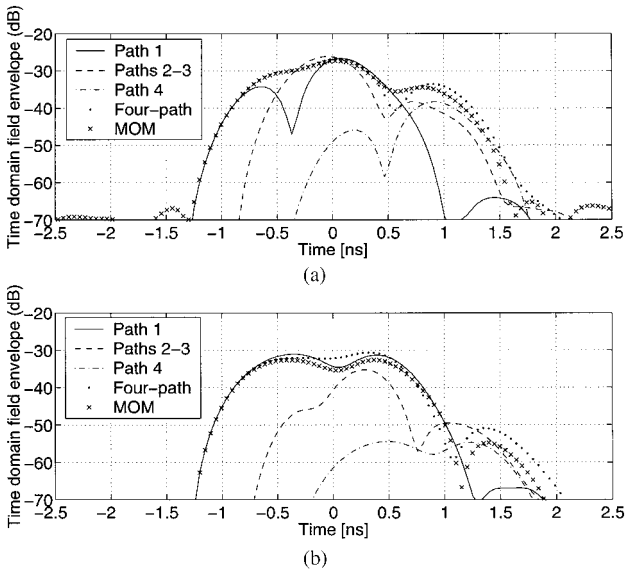

Figure 6 Envelope of time-domain backscattered fields for 45° incidence. Comparison of method of moments with four-path model. (a) *HH*. (b) *VV*

Several higher order object–surface interaction mechanisms can be proposed to explain these differences. In particular, a path in which the incident field is scattered by the target into a direction propagating normally onto the half space, reflected, and then rescattered by the object into the backscattering direction would produce contributions around time zero. Multiple reflections between the bottom surface of the target and the half space would then appear at later times, beginning with the approximate time of path 4. Each proposed higher order mechanism also has a corresponding set of four-paths, leading to further time-delayed contributions.

6. CONCLUSIONS

The results of this paper demonstrate that the basic premise of the four-path model for scattering from an object above a half space is valid, but that higher order effects can be significant in some cases which reduce four-path model accuracy. Clearly, the geometry of the target and its location relative to the half space will play an important role in the relevance of higher order mechanisms; the example illustrated here is one for which higher order interactions should be moderately strong. Time-domain backscattered returns allowed four-path model terms to be distinguished, and showed higher order mechanisms to become more important as time delays increase.

ACKNOWLEDGMENT

Discussions with Dr. R. J. Burkholder and Dr. P. H. Pathak are appreciated. Use of the IBM SP system at the Maui High Performance Computing Center is acknowledged, sponsored by the Air Force Research Laboratory, Air Force Material Command under cooperative agreement F29601-93-2-0001. Opinions, interpretations, conclusions, and recommendations are those of the authors, and are not necessarily endorsed by the United States Air Force, Air Force Research Laboratory, or the U.S. Government.

REFERENCES

1. L. Tsang, J.A. Kong, and R.T. Shin, Theory of microwave remote sensing, Wiley, New York, 1985.
2. E.A. Shtager, An estimation of sea surface influence on radar reflectivity of ships, IEEE Trans Antennas Propagat 47 (1999), 1623–1627.
3. M.A. Sletten, D.B. Trizna, and J.P. Hansen, Ultrawide-band radar observations of multipath propagation over the sea surface, IEEE Trans Antennas Propagat 44 (1996), 646–651.
4. T. Chiu and K. Sarabandi, Electromagnetic scattering interaction between a dielectric cylinder and a slightly rough surface, IEEE Trans Antennas Propagat 47 (1999), 902–913.
5. J.Q. He, T.J. Yu, N. Geng, and L. Carin, Method of moments analysis of electromagnetic scattering from a general three-dimensional dielectric target embedded in a multilayered medium, Radio Sci 32 (2000), 305–313.
6. N. Geng, M.A. Ressler, and L. Carin, Wide-band VHF scattering from a trihedral reflector situated above a lossy dispersive half-space, IEEE Trans Geosci Remote Sensing 37 (1999), 2609–2617.
7. T.J. Cui and W.C. Chew, Fast algorithm for electromagnetic scattering by buried 3-D dielectric objects of large size, IEEE Trans Geosci Remote Sensing 37 (1999), 2597–2608.
8. J.T. Johnson and R.J. Burkholder, Coupled canonical grid/discrete dipole approach for computing scattering from objects

above or below a rough interface, IEEE Trans Geosci Remote Sensing (2000, accepted).
9. R. Barrett, M. Berry, T. Chan, J. Demmel, J. Donato, J. Dongarra, V. Eijkhout, R. Pozo, C. Romine, and H. van der Vorst, Templates for the solution of linear systems: Building blocks for iterative methods, available by ftp from netlib2.cs.utk.edu, 1993.
10. L. Tsang, C.H. Chan, K. Pak, and H. Sangani, Monte Carlo simulations of large scale problems of random rough surface scattering and applications to grazing incidence with the BMIA/canonical grid method, IEEE Trans Antennas Propagat 43 (1995), 851–859.
11. J.T. Johnson, R.T. Shin, J.A. Kong, L. Tsang, and K. Pak, A numerical study of the composite surface model for ocean scattering, IEEE Trans Geosci Remote Sensing 36 (1998), 72–83.
12. B.T. Draine and P.J. Flatau, Discrete-dipole approximation for scattering calculations, J Opt Soc Amer A 11 (1994), 1491–1499.
13. P.J. Flatau, Improvements in the discrete-dipole approximation method of computing scattering and absorption, Opt Lett 22 (1997), 1205–1207.
14. K. Pak, L. Tsang, C.H. Chan, and J.T. Johnson, Backscattering enhancement of electromagnetic waves from two dimensional perfectly conducting random rough surfaces based on Monte Carlo simulations, J Opt Soc Amer 12 (1995), 2491–2499.
15. Maui High Performance Computing Center World Wide Web Site, on the World Wide Web at www.mhpcc.edu.
16. E. Newman, A user's manual for the electromagnetic surface patch code: Preliminary version ESP5.0, ElectroScience Laboratory, The Ohio State University, unpublished rep, 1997.

TWO INTEGRATED STACKED SHORTED PATCH ANTENNAS FOR DCS / WLAN DUAL-BAND OPERATIONS

Jian-Yi Wu[1] and Kin-Lu Wong[1]
[1] Department of Electrical Engineering
National Sun Yat-Sen University
Kaohsiung, Taiwan 804, R.O.C.

Received 7 February 2001

ABSTRACT: *A new design of two stacked shorted patch antennas integrated on the same microwave substrate for DCS and WLAN dual-band operations is presented. The two antennas together occupy a small area of 19 × 28.5 mm², and the heights for the DCS and WLAN antennas are 10 and 5.2 mm, respectively. Details of the measured antenna performances are presented.* © 2001 John Wiley & Sons, Inc. Microwave Opt Technol Lett 30: 134–136, 2001.

Key words: *stacked shorted patch antenna; dual-band operation; DCS operation; WLAN operation*

1. INTRODUCTION

Stacked shorted patch antennas can have enhanced impedance bandwidths compared to a regular single-layer shorted patch antenna, and several promising designs have been reported [1–3]. These available designs, however, are mainly for single-band operation. In this paper, we present a new design for integrating two stacked shorted patch antennas on the same microwave substrate to perform DCS (digital communication system, 1710–1880 MHz) and WLAN (wireless local-area network, 2400–2485 MHz) operations. The two antennas, having separate feeding ports, are integrated in a compact configuration, and meet the bandwidth requirements for the DCS and WLAN operations, respectively. Details of the antenna design are described, and experimental results of a constructed prototype are presented and discussed.

2. ANTENNA DESIGN

Figure 1 shows the proposed compact configuration of two stacked shorted patch antennas for DCS and WLAN operations. The side views of the DCS and WLAN antennas are, respectively, shown in Figure 1(a) and (b). Figure 1(c) depicts the top view of the integrated configuration of the two antennas, whose lower or driven patches are printed on the same microwave substrate (thickness 3.2 mm and relative permittivity 4.4 in this design) and short circuited to the same ground plane through the microwave substrate. Six and four shorting pins, symmetrically arranged close to the two ends of the shorted edge, are used for short circuiting the lower patches of the DCS and WLAN antennas to the ground plane, respectively. On the other hand, the upper or parasitic patches of the two antennas are short circuited to the same ground plane using a single shorting pin at the center of the shorted edge. The region between the shorted lower and upper patches is an air layer, and plastic posts (not shown in the figure) are used for supporting the upper patch above the lower one. Also note that separate coax feeds are used for the two antennas, and the feed position is selected along the center line of the lower patch.

In order to achieve a compact integrated configuration for the two antennas, the lower patch of the DCS antenna is transformed to have an L shape, which effectively reduces the required lower patch length to be 19 mm (without the patch shape transformation, the required lower patch is about 23 mm), and placed close to that of the WLAN antenna with a small gap of 2 mm. This arrangement makes the two antennas together occupy a small area of 19 × 28.5 mm². As

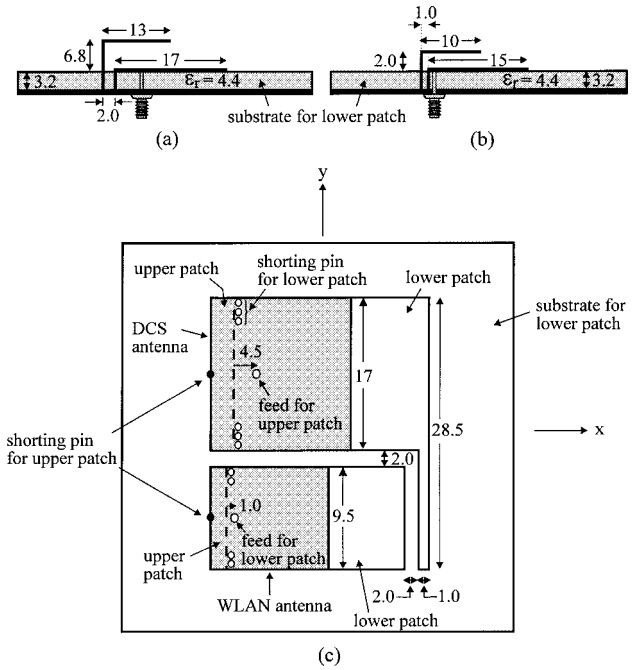

Figure 1 (a) Side view of the stacked shorted patch antenna for DCS operation. (b) Side view of the stacked shorted patch antenna for WLAN operation. (c) Top view of the DCS and WLAN antennas integrated on the same microwave substrate. Dimensions given in the figures are in millimeters, and the ground-plane size is 50 × 50 mm²